CAMBRIDGE
UNIVERSITY PRESS

Circularly polarized diversified MIMO antenna design for millimeter-wave on-body applications using characteristic mode theory

Sumon Modak[1] , Anjaneyulu Lokam[1] and Umar Farooq[1,2]

[1]Department of Electronics and Communication Engineering, National Institute of Technology Warangal, Telangana, India and [2]Department of Electronics and Communication Engineering, VNR Vignana Jyothi Institute of Technology Hyderabad, Telangana, India

Abstract

This paper presents a systematic design approach for developing a semiflexible multiple-input–multiple-output antenna system operating in the millimeter wave frequency spectrum, specifically designed for body-worn applications in biotechnologies. The designed antenna features dual flower-shaped antenna radiators placed in a spatial diversity configuration. Strategic modifications have been implemented by integrating dual crescent-shaped slots in the ground layer to attain the targeted frequency band of 25.7–30.6 GHz. Later, the upper edge of the ground plane is truncated in order to achieve circularly polarized radiation characteristics at 29.4 GHz with 3 dB ARBW of 0.6 GHz (29.1–29.7 GHz). The realization of circular polarization in the antenna geometry is validated through the analysis of characteristic mode theory. A maximum gain of 5.6 dBi is attained along with a port isolation of >30 dB. The proposed antenna undergoes analysis to assess its performance in the bending conditions and specific absorption rate, besides validation of diversity metrics encompassing envelope correlation coefficient, diversity gain, channel capacity loss, total active reflection coefficient, and mean effective gain has also been conducted. Finally, the proposed antenna structure is fabricated, and its performance is validated and subsequently compared with that of its simulated counterpart.

Introduction

Over the years the progression of wireless technology has precipitated a notable rise in the utilization of body-centric wireless communication. This development has gained considerable attention from researchers globally, owing to its diverse application across various domains including healthcare, household, sports, military operation, and internet of things (IoT) [1–3]. In regards to that antenna serves as an essential component that facilitates wireless connectivity and plays a key role in body centric wireless network applications. Among various antennas, microstrip antennas stand out as the preferred option in the research community for their prominent adaptability, minimal weight, user-friendly design, and cost-effectiveness [4, 5]. Notably, wearable antennas designed for body-worn applications required inherent flexibility to effectively conform to the contours of human body parts. This feature not only ensures a suitable fit but also minimizes the risk of collision with other rigid objects [6]. Considerable progress has been achieved in the advancement of adaptable antenna configurations tailored for diverse wearable applications. A novel textile-based wearable antenna, suitable for medical and IoT applications has been introduced in reference [7]. Likewise utilizing polyester substrate a metamaterial-based wearable antenna is conceptualized to operate at 5.1 GHz for WLAN applications [8]. A multilayer antenna design, utilizing textile and felt substrates, is developed for wearable applications, operating at 2.45 and 3.4 GHz with high gain (5.1 and 8.6 dBi), and low SAR (0.2 and 0.1 W/Kg) [9]. Two different configurations of ultrawide band antenna intended for wearable applications are detailed in references [10, 11]. Furthermore, the realization of the proposed antenna structure is examined through various scenarios, including assessment under coaxial feeding conditions, bending, and evaluation of specific absorption rate (SAR) levels. In reference [12] a flexible, flower-shaped antenna is designed by integrating rounded slots, parasitic elements, and a modified ground layer. The reported antenna delivers an expansive bandwidth of 2.86 GHz (3.43–6.29 GHz) and a peak gain of 3.7 dBi. Additionally, bending analysis was conducted to evaluate the flexibility of the prototype. It is worth mentioning that the bending effect in the antenna structure introduces considerable challenges to maintain robust communication links. This is primarily due to the reflection and scattering of electromagnetic (EM) waves while being propagates across the curved body surface [13, 14]. Moreover, the bending

challenge faced by wearable antennas is unavoidable. Therefore to effectively address this issue multi-input–multi-output (MIMO) antenna emerges as a viable solution. The antenna designs detailed in references [15–31] are tailored for body-worn applications, specifically focusing on dual and quad-port MIMO systems. In reference [15] a nonconventional leather material is used to design a dual-port MIMO antenna system operating over a broad frequency range of 2.2–8 GHz with a fractional bandwidth of 113%. A novel MIMO antenna system has been developed employing characteristic mode theory (CMT) [16]. The design incorporates a compact ground plane as the principal radiator, supplemented by capacitive loaded strips. This configuration enhances the antenna's impedance bandwidth by up to 20%. A flexible four-port wearable MIMO antenna structure capable of operating across a wide frequency range from 2–14 GHz with isolations of 15 dB is presented by Jayant et al. [17]. In the realm of wearable technology, a four-port MIMO antenna system has been tailored to operate across three distinct frequency bands of 2.54–3.56 GHz, 4.28–4.97 GHz, and 5.37–8.85 GHz respectively [18]. In reference [19] utilizing jeans textile material quad element MIMO antenna system functioning over a frequency range of 2.9–4.1 GHz with an isolation of 19 dB is designed for wearable 5G technology. Noteworthy MIMO designs incorporating circular polarization (CP) enhance communication robustness by reducing the polarization loss and mitigating multipath interference. This is particularly advantageous during the mobility of individuals wearing the wearable device [20, 21]. Two different configurations of novel circularly polarized dielectric resonator MIMO antennas have been designed and investigated for WBAN and 5G wireless applications. The first antenna operates within the frequency band of 6.8–8.9 GHz [22], while the second targets the millimeter-wave band of 25.4–31.8 GHz [23]. Both configurations achieve impressive axial ratio bandwidths (ARBWs) of 11.5% and 11%, along with remarkable isolation values of 22 and 25 dB respectively. Textile-based MIMO antenna design, featuring two sickle-shaped resonators is explored in reference [24]. The ground plane incorporates inverted L-shaped strips to facilitate CP. A miniaturized circularly polarized MIMO antenna system for wearable biotelemetric devices has been designed to operate efficiently across a wide frequency bandwidth of 2.23 GHz [25]. In reference [26], a dual-port MIMO antenna system featuring L-shaped radiator is presented. Additionally, a Z-shaped slot is incorporated into the ground plane to achieve left- and right-hand circularly polarized radiation patterns. Nevertheless, these antennas have typically been constrained by limited operational bandwidth, sizable system volumes, and a lack of design optimization for operation within millimeter-wave frequency band. In regard to that, a novel circularly polarized MIMO antenna has been designed to operate efficiently at 37.8 and 50 GHz, demonstrating enhanced isolation of −25 dB and excellent diversity performance [27]. Authors in reference [28] proposed a dual-port MIMO antenna system operating across four distinct frequencies of 16, 25.5, 28, and 32 GHz within millimeter-wave frequency spectrum applicable for 5G, beyond 5G, and future 6G communications. A novel strategy incorporating a 5×5 electromagnetic bandgap unit cell configuration has been proposed beneath the antenna structure to reduce back radiations. The suggested structure is a two-port MIMO antenna system optimized for operation at 24 GHz, thereby rendering it well-suited for millimeter-wave wearable applications [29]. A cutting-edge multiport antenna system has been engineered for wearable biotechnology applications, operating seamlessly across a wide frequency spectrum spanning from 24 to 31 GHz. Remarkably, it achieves isolation levels up

to 40 dB [30]. Shariff et al. [31] presented a quad-port MIMO antenna system working at 30.5 GHz. Additionally, a T-shaped decoupling configuration has been implemented to augment the isolation among antenna elements. Although significant efforts have been dedicated to the development of MIMO antenna designs tailored for wearable applications [15–31]. Despite these endeavors, such designs are affected by several inherent limitations. These limitations notably encompass bulky physical dimensions [15–17, 19, 22–26, 28], restricted operational frequency ranges [16, 18, 19, 22, 25, 26, 29], low gain [15, 16, 18, 19, 22, 25, 29, 30], and also shortcomings in achieving satisfactory levels of circularly polarized radiation behavior. Further, the analysis of SAR and bending were missing in references [16, 18], and references [22–25]. Moreover, there exists a scarcity of literature addressing the application of the CMT in the design of antenna structures, particularly in the context of millimeter-wave wearable MIMO antenna designs. This gap highlights the need for further exploration in this domain. Hence to address these challenges, this letter presents the design of a novel circularly polarized dual-element MIMO antenna system. The design leverages an in-depth analysis based on the CMT, enabling the antenna to achieve circularly polarized radiation characteristics. The recommended antenna system features a unique flower-shaped geometry, which is an optimized modification of a conventional circular antenna structure. This innovative design achieves a wide operational frequency bandwidth of 4.9 GHz, ranging from 25.7 to 30.6 GHz, and also offers a notable maximum gain of 5.6 dBi. In addition, the suggested antenna design ensures excellent mutual coupling between ports, with an impressive isolation of up to −34 dB. To further validate the suitability of the proposed antenna for wearable applications, comprehensive on-body performance evaluations, including bending tests and SAR analysis, have been conducted. These evaluations demonstrate the robustness of the antenna's performance under realistic conditions, confirming its potential for practical deployment in body-worn communication systems operating in the millimeter-wave frequency bands.

Antenna geometrical configurations

The geometrical outline and the effective design parameters for the proposed dual element MIMO antenna system is shown in Fig. 1. Where Fig. 1(a) illustrates the top view, and the bottom view is shown in Fig. 1(b). The geometry features flower shaped antenna radiators, with each element comprising five petals (minor and major radius $r2$ and $r3$) and fed by a 50 Ω transmission line. The antennas are organized in a spatial diversity configuration, where in identical elements are positioned adjacent to each other with a gap of D1 (Fig. 1(a)). The bottom side of the substrate hosts two crescent shaped defected ground structures. Subsequently, the upper edge of the ground plane is truncated as part of an enhancement strategy to improve performance. The reported MIMO antenna structure is designed over a semiflexible Rogers 5880 substrate, with dimensions measuring $32 \times 20 \times 0.508$ mm^3. The additional optimized dimensions are as follows: $Ls = 32$ mm, $Ws = 20$ mm, $D1 = 6.35$ mm, $Wf = 2.1$ mm, $Lf = 11.37$ mm, $r1 = 3.5$ mm, $r2 = 2$ mm, $r3 = 4$ mm, $R1 = 5$ mm, $G1 = 0.57$ mm, $L1 = 12.36$ mm, $L2 = 5.29$ mm. ANSYS HFSS tool is used for the design and simulation process.

The development of the recommended MIMO antenna structure and its associated design stages are depicted in Fig. 2. The simulated S-parameters, total gain, and axial ratio (AR) are shown in Fig. 3(a–d). The first step in the design process involves
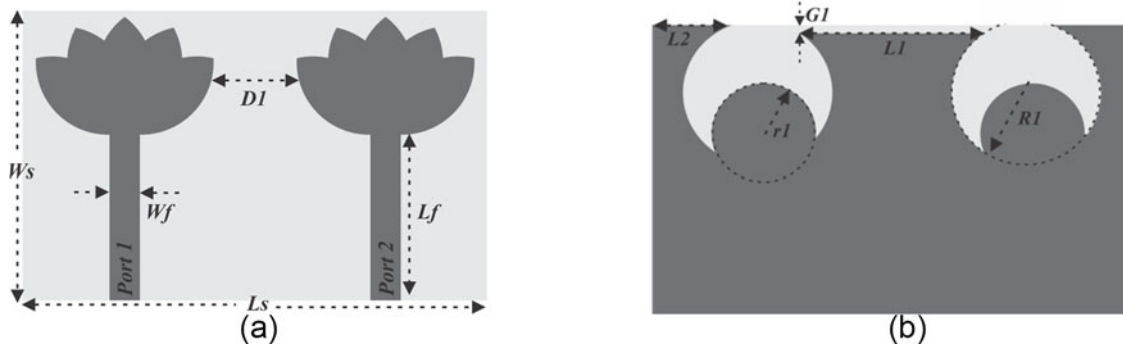
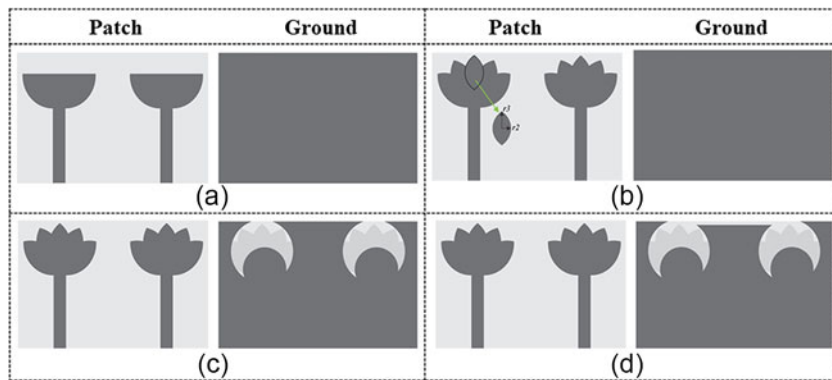**Figure 1.** Geometrical configurations (a) Top-view, (b) Bottom-view.

Figure 2. Design steps (a) Ant_I, (b) Ant_II, (c) Ant_III, (d) Ant_IV (proposed).

conceptualizing a reference circular monopole antenna with its initial dimension of radius 6.1 mm, derived from reference [32]. Subsequently, the circular radiator is modified into a semicircular structure to achieve the desired frequency response. However, for the sake of brevity, the first design step is not discussed in detail. Here the initial design stage starts with the development of a dual-element semicircular radiating patch with a complete ground plane stated as Ant_I (See Fig. 2(a)). This configuration demonstrates a nonzero resonant mode viz. TM_{21} at 28.2 GHz, showing $|S_{11}|$ value of approximately −6 dB. This validation is confirmed by examining the impedance plot of a single element of Ant_I (see Fig. 4(a)). Utilizing equation (1) the nonzero resonant frequency (f_r) for Ant_I is computed and found to be 27.6 GHz [33].

$$f_r = \frac{K_{nm}v_0}{2\pi R\sqrt{\varepsilon_r}} \qquad (1)$$

Where, "v_0" represents the velocity of light in vacuum, "R" = 6 mm refers to the radius of a semicircular patch along the horizontal direction, $K_{nm} = 5.135$ signifies the root of the derivative of the Bessel function. In order to enhance the impedance matching within the desired frequency bands of interest (25–31 GHz), Ant_I is modified by inserting five petal-shaped parasitic stubs, placed strategically overlapped to each other on both the antenna radiators, resulting in distinctive flower-shaped antenna structure. However, the ground layer remains intact. This configured antenna structure (Ant_II) improves the impedance matching. The same has been validated through the surface current distribution plot. Figure 4(b) indicates the current with higher intensity is concentrated along the upper periphery of the flower petals (marked with

a circle). Conversely, minimal current density is observed at the center of the patch.

Notably, a similar current distribution pattern is maintained across other antenna element (port 2) due to their identical characteristics. From this observation it can be concluded that most of the radiations occur from the upper periphery of the flower petals, thereby establishing resonance at 27.5 GHz, with an impedance bandwidth extending from 27.3 to 27.8 GHz, which can be seen from Fig. 3(a). Although Ant_II is capable of providing a zero resonant frequency with 0.5 GHz bandwidth. However, the primary goal remains the attainment of wideband characteristics within 25–31 GHz band. To accomplish this, alterations have been made to the ground plane of Ant_III, involving the integration of a crescent-shaped slot. The crescent-shaped defected ground plane is designed by integrating circular defected ground structures (having radius $R1$). Later, a small circular conductor with a radius "$r1$" is strategically positioned over each defected ground structure, while the top layer of the antenna remains unchanged (See Fig. 2(c)).

Moreover, it is widely recognized that incorporating slots over the antenna radiator or ground layer can enhance operational bandwidth. Nevertheless, this practice significantly impacts the antenna's radiation characteristics and gain [34, 35]. With these modifications, Ant_III provides an expanded operational bandwidth spanning from 25.3 to 30.1 GHz, with a remarkable coupling level of −30 dB. Noted, this modification results in a reduction in antenna gain to 3.5 dBi (see Fig. 3(c)). An investigation into resonance and gain is undertaken through a parametric study involving the variation of the radius "$r1$" (small circle). The observation from Fig. 5(a) illustrates that as the parameter "$r1$" increases; there is a noticeable enhancement in antenna impedance matching.
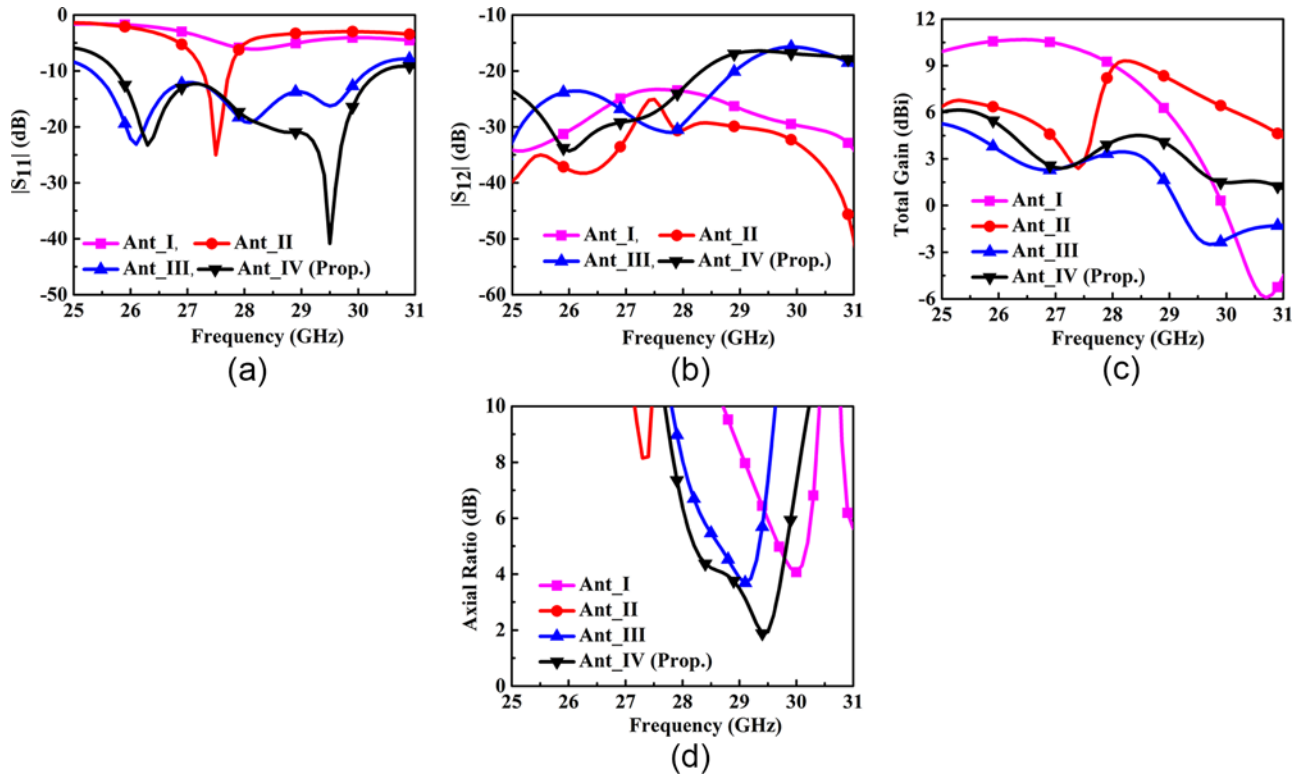
Figure 3. Performance evaluation (a) $|S_{11}|$, (b) $|S_{12}|$, (c) Total gain, (d) Axial ratio.
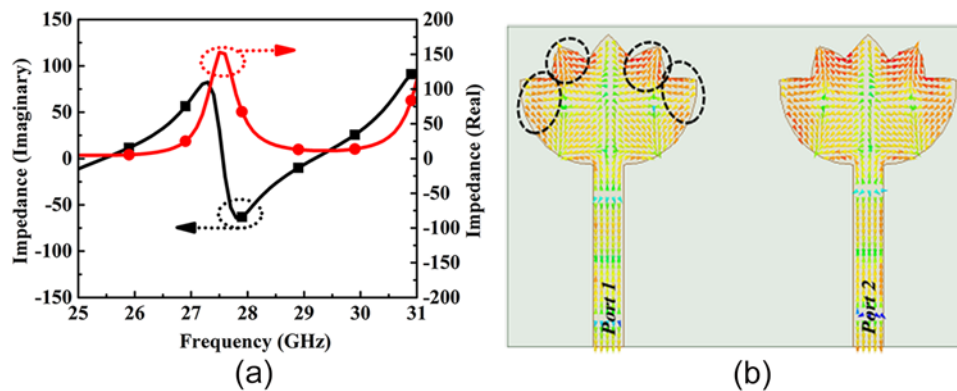
Figure 4. (a) Plot of impedance, (b) Surface current density at 27.5 GHz.

This improvement continues until "$r1$" reaches a value of 3.5 mm, beyond which the impedance begins to degrade. Similarly, when comparing gains within the desired band, it becomes apparent that except for the case where $r1 = 3.5$ mm, the values of "$r1$" exhibit negative gains. Despite the aforementioned findings, further modifications have been implemented within the ground layer to attain circularly polarized (CP) radiation characteristics. This realization of the same has been thoroughly analyzed utilizing the CMT. It is well documented in existing literature that generating circularly polarized (CP) radiation requires the simultaneous excitation of two orthogonal characteristic modes with a 90° phase difference. This entails that the characteristic angles of these modes should ideally be characteristics angle (CA)1 = 135°, and CA2 = 225°, thereby deviating by 45° from the resonance angle of 180°. Besides, both modes should possess identical modal significance (MS) values, ensuring MS1 = MS2

[36, 37]. Considering this, the ground layer of Ant_III has been modified by truncating the upper edges by a width of $G1$ (see Fig. 2(d)).

Now to investigate the modal behavior satisfying the CP condition, modal analysis has been sorted at a frequency of 29 GHz and is carried out utilizing the CST Microwave studio tool. The analysis of MS highlights the significance of all modes M1–M4. Specifically, M1 and M2 resonate distinctly at frequencies of 29.49 and 29.57 GHz, respectively. Conversely, M3 and M4 coincide, resonating at a common frequency of 28.65 GHz, with an associated MS value of 1 as illustrated in Fig. 6(a). At a frequency of 29.27 GHz, it has been noted that the magnitudes of modes M1–M4 coincide. This observation suggests that, at 29.27 GHz, the CA values between the modes exhibit a phase difference of 92°. This has been validated through the CA curves depicted in Fig. 6(b), where modes M1 and M3, M1 and M4, M2 and M3, and M2 and
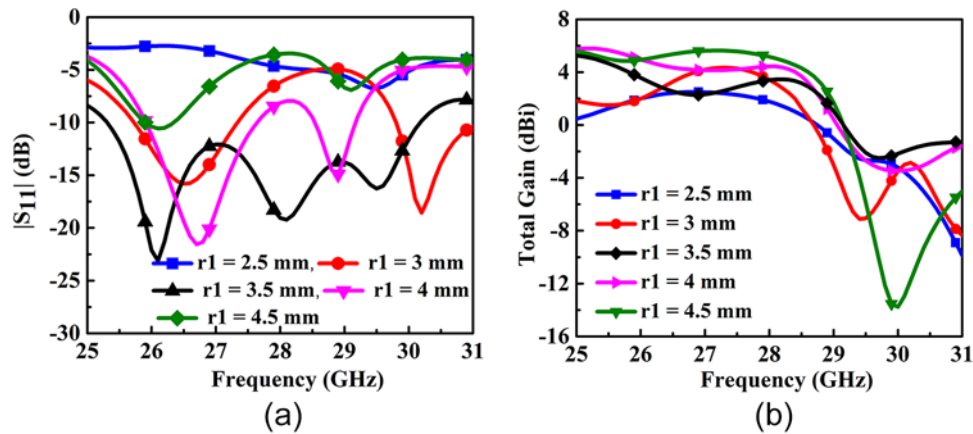
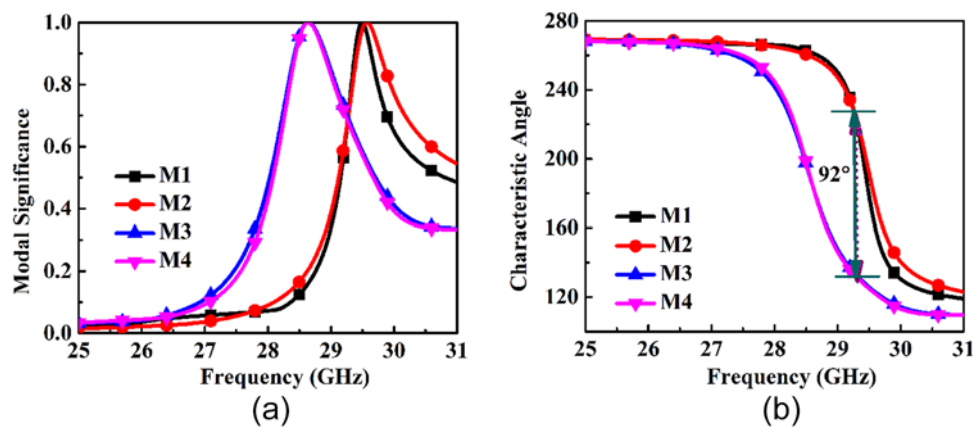**Figure 5.** Parametric variations (a) |S₁₁|, (b) Total gain.

Figure 6. Mode analysis (a) Modal significance, (b) Characteristic angle.

M4 exhibit a phase difference of almost 45° from the resonance angle of 180°. (CA1 and CA2 = 226°, CA3 and CA4 = 134°). The modal current distributions (J_1 and J_3, J_1 and J_4, J_2 and J_3, J_2 and J_4) corresponding to modes M1 and M3, M1 and M4, M2 and M3, and M2 and M4 are illustrated in the Fig. 7. Notably, it is evident that the current distributions in modes J_1 and J_3, J_1 and J_4, J_2 and J_3, and J_2 and J_4, exhibit a high degree of orthogonality, as indicated with black arrow. However, an exception arises at mode M2, where the current flows in the opposite direction, highlighted with red color. From the 3D radiation patterns, it can be seen that only J_1 & J_4 radiate almost in all directions, whereas, J_2 radiates in ±y direction having null in ±z direction, and J_3 radiates in ±x direction (see Fig. 7(a-d)).

Finally, the assessment conducted using CMT confirms that by truncating the ground layer, Ant_IV demonstrates the ability to generate a significant phase difference of 92° across various modes, effectively achieving CP properties at 29.4 GHz with a 3 dB ARBW spanning from 29.1 to 29.7 GHz. Additionally, a parametric analysis is conducted to evaluate the circularly polarized radiation characteristics by varying the width "G1" of the truncated section on the ground layer. From Fig. 8, it is evident that at G1 = 0.4 mm, the antenna does not exhibit circularly polarized radiation behavior. However, at G1 = 0.8 mm, an ARBW of 0.3 GHz (29.1–29.4 GHz) is achieved. Further increasing G1 = 1 mm results in a reduction of ARBW to 0.2 GHz (29.2–29.4 GHz). This analysis reveals that as the width "G1" increases, the ARBW decreases.

Therefore, the optimized dimension for G1 is determined to be 0.57 mm. Finally, the proposed antenna (Ant_IV) showcases a broad operating bandwidth extending from 25.7 to 30.6 GHz making it well-suited for body-centric applications in the healthcare domain. The simulated performances of all design iterations (from Ant_I to Ant_IV) are outlined in Table 1 for comparative analysis.

Conformability and on-body performance analysis

In wearable technology contexts, it is crucial to conduct the analysis because the configuration of the suggested antenna structure may be bent with the body's contours when positioned on various parts of human body, such as the hand, and biceps, potentially altering its performance characteristics. This assessment entails the evaluation of performance under conditions where the antenna structure is subjected to bending along the Y-axis, with radii "Ry" as depicted in Fig. 9. Figure 10(a) illustrates the comparison of the simulated |S₁₁| values. The findings demonstrate the robustness of the suggested wearable antenna, particularly in relation to its overall impedance bandwidth across various bending radii. Nevertheless, at a bending radius Ry = 15 mm, the antenna impedance gets mismatched. This is due to the decrease in effective resonating length caused by increased bending.

Similarly, it has also been observed that at Ry = 30 mm the resonance is shifted toward the lower frequency. The analysis also
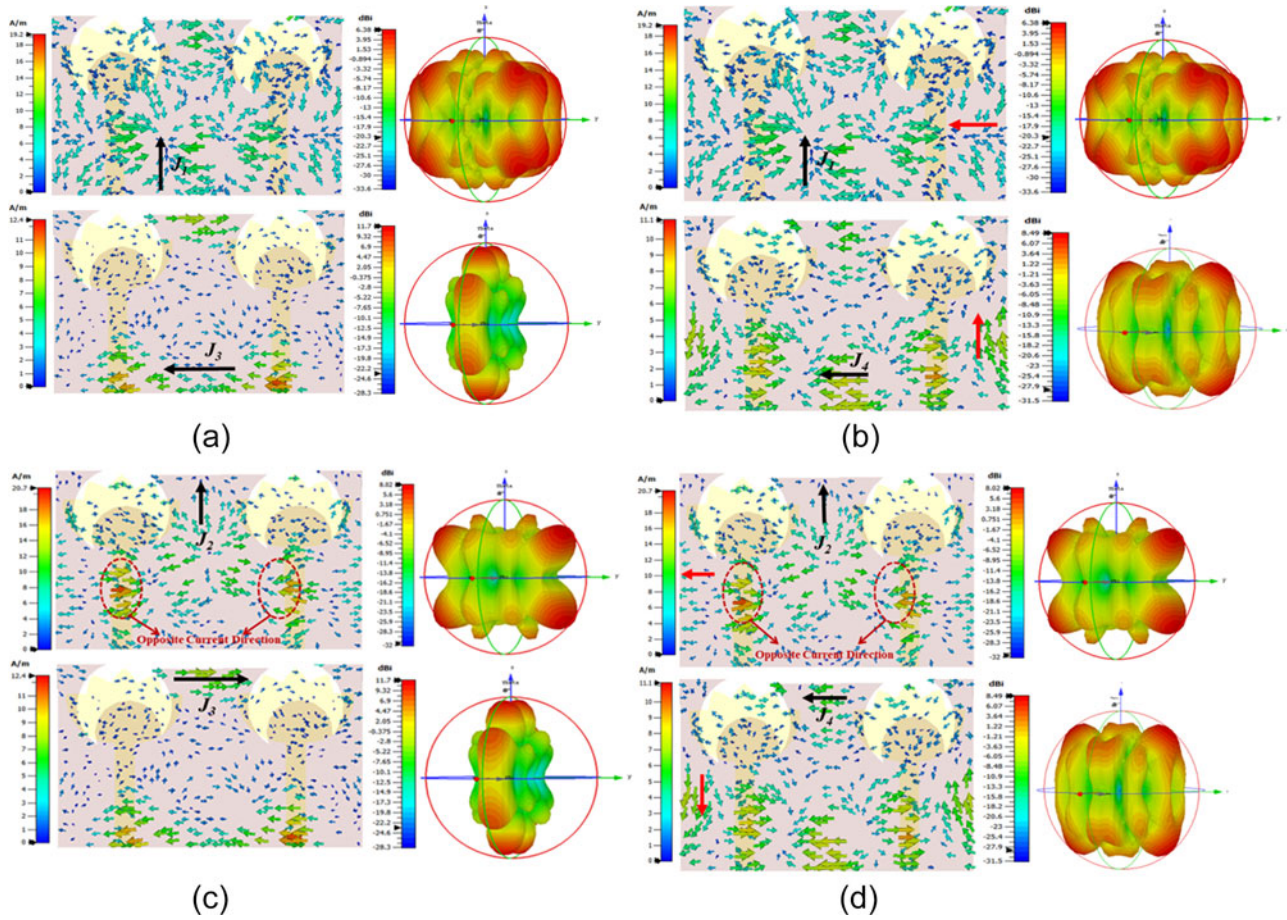
Figure 7. Modal current distributions (a) J_1 & J_3, (b) J_1 & J_4, (c) J_2 & J_3, (d) J_2 & J_4.
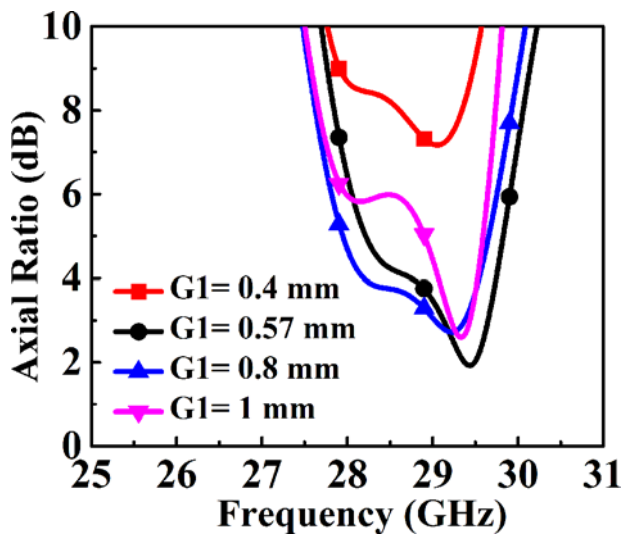

Figure 8. Parametric analysis corresponds to width G1.

Table 1. Design iterations performance comparisons

	Ant_I	Ant_II	Ant_III	Ant_IV (Prop.)
Resonant frequency (GHz)	28.2	27.5	26.1, 28.1	26.2, 29.5
Return loss (dB)	−6	−25	−20	−23
Operating bands (GHz)	NA	27.3–27.8	25.3–30.1	25.7–30.6
Max. $|S_{12}|$ (dB)	NA	−25	−31	−34
Max. gain (dBi)	NA	9.3	4.8	5.6
Axial ratio bandwidth (ARBW)	NA	NA	NA	29.1–29.7

it is crucial to assess the characteristics of the antenna, including its S-parameters ($|S_{11}|$/$|S_{12}|$), and SAR, under wearable conditions. In this context, the antenna is positioned on a human body tissue model composed of three layers, including the skin ($\varepsilon_r = 16.6$, $\sigma = 25.8$), fat ($\varepsilon_r = 6.09$, $\sigma = 5.04$), and muscle ($\varepsilon_r = 24.4$, $\sigma = 33.6$), arranged in a cubic configuration with an overall size of $32 \times 28 \times 15$ mm^3. Noteworthy, the antenna-to-skin surface distance is maintained at 6 mm (h) which resembles the thickness of the cloth [30].

The electrical properties of different tissue layers are characterized with respect to a frequency of 28 GHz. The radiation

extends the 3 dB ARBW of the proposed MIMO antenna across various bending conditions, as illustrated in Fig. 10(b). Notably, regardless of the values of Ry, the designs consistently exhibit circularly polarized radiation patterns across the operational frequency range. As the antenna is intended for on-body applications
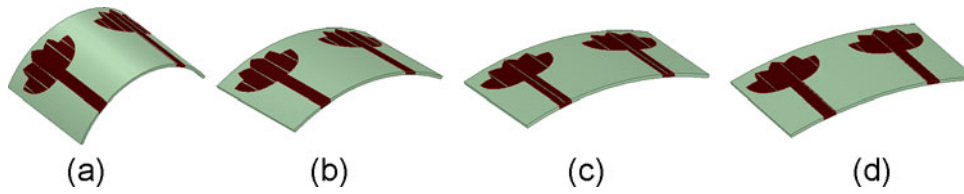
Figure 9. Bending radii Ry (a) 15 mm, (b) 30 mm, (c) 45 mm, (d) 60 mm.
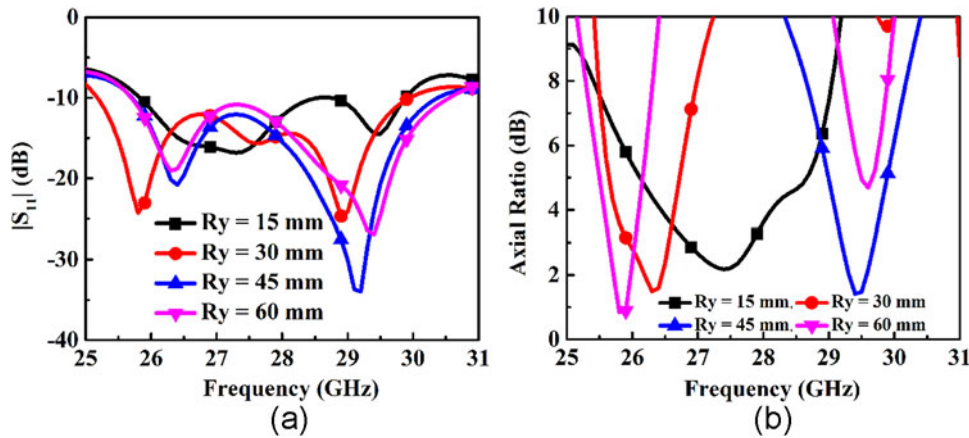

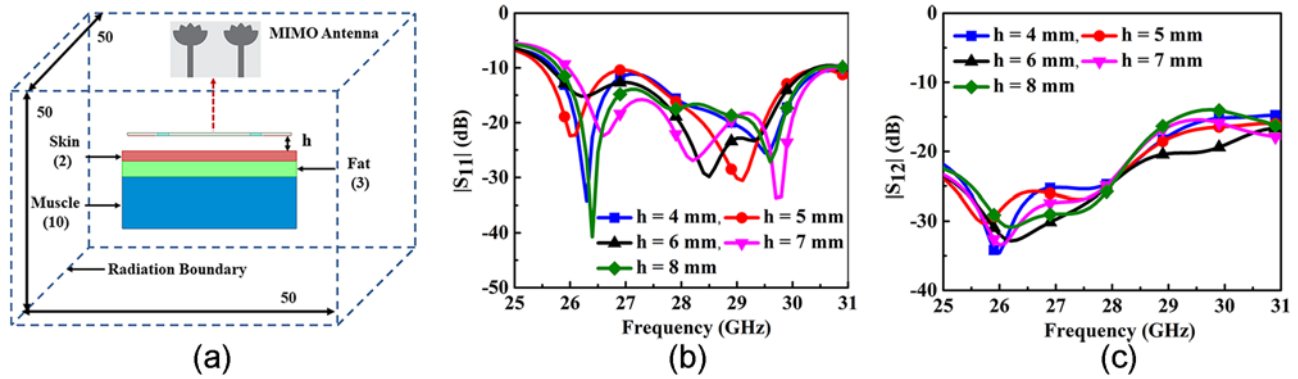**Figure 10.** Performance evaluation (a) $|S_{11}|$, (b) Axial ratio.

Figure 11. Performance comparison with respect to height (h) (a) Human body tissue model, (b) $|S_{11}|$, (c) $|S_{12}|$.

boundaries are maintained at a significant distance $\gg \lambda_0/2$ (See Fig. 11(a)). Figure 11(b) illustrates the simulated $|S_{11}|$, indicating impedance mismatch occurring at 27 GHz for $h = 4$ and 5 mm. Simultaneously, with increasing height (h), antenna performance shows improvement. Likewise, it can also been noted that varying the height (h) does not significantly impact the performance of $|S_{12}|$. The assessment of SAR has been conducted, focusing on ensuring human safety. Currently, there are no established standards for accessing SAR at millimeter-wave frequency spectrums. Therefore, the validation of the proposed MIMO antenna is being conducted by adhering to existing guidelines set forth by regulatory bodies such as the Federal Communications Commission, and International Commission on Non-Ionizing Radiation Protection [31]. The average specific absorption rate is witnessed to be 2.59 and 2.2 W/kg at a frequency of 28 and 30 GHz respectively, when subjected to an input power level of 100 mW through a single antenna element (see Fig. 12). To comply with the upper SAR limit, the maximum allowable power that can be delivered to the proposed antenna is 72 mW.

Experimental analysis

Fabricated prototype

This section discusses the efficacy of the suggested antenna design that has been substantiated through rigorous experimental measurements. The fabrication of the proposed antenna system is executed on a Rogers RT/duroid 5880 substrate employing a precise photolithographic etching process. Figure 13(a-b) depict the top and bottom views, respectively, of the fabricated antenna prototype. The antenna structure is excited by attaching a 2.92 mm end launch jack, screw on female socket connector 145-0711-802, up to 40 GHz (Johnson/Cinch connectivity solutions) which is linked with Anritsu MS46122B vector network analyzer for accessing S-parameters across various ports (see Fig. 13(c)). The comparison between simulated and measured $|S_{11}|$/$|S_{22}|$, and $|S_{12}|$ in a free-space scenario reveals a close alignment within the millimeter-wave frequency spectrum. The measured impedance bandwidth is observed to be 26–30.4 GHz ($|S_{11}|$), 25.6–30.5 GHz ($|S_{22}|$), and having a maximum isolation of −31 dB
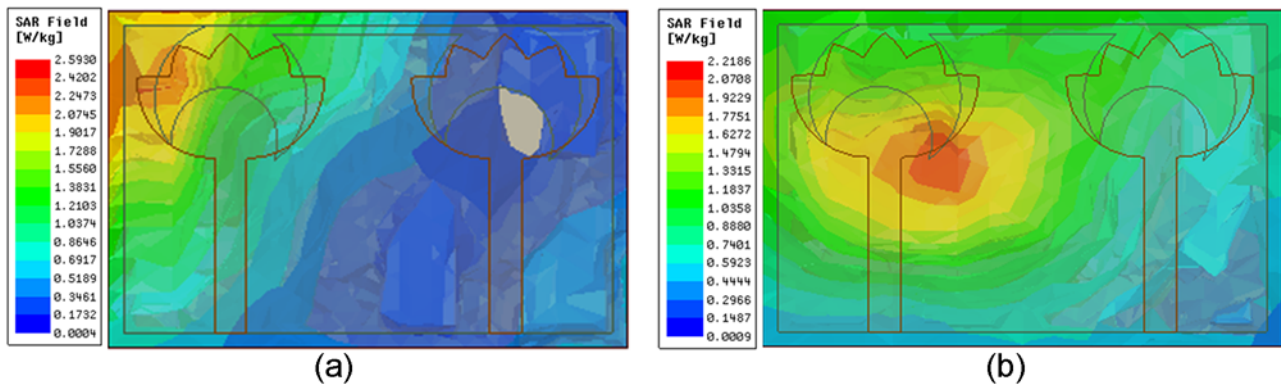
Figure 12. Specific absorption rate (a) 28 GHz, (b) 30 GHz.
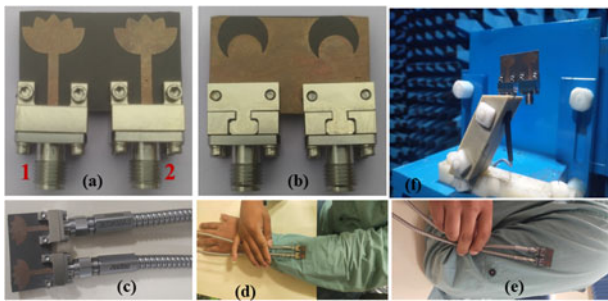
Figure 13. Fabricated prototypes and experimental setups.

($|S_{12}|$) shown in Fig. 14(a). Similarly, the practical viability of the proposed antenna's adaptable characteristics for real-time applications is effectively demonstrated through the placement of the antenna structure on the hand and biceps (see Fig. 13(d, e)). Figure 14(b) presents a comparison of the measured behavior of S-parameters.

It is obvious that in the case of on-hand and on-biceps scenarios, the first resonance frequency is subtly shifted toward lower frequency bands. Additionally, a slight impedance mismatch is observed when compared to the simulated value at 26.8 GHz. This has been attributed to the elevated permittivity characteristic of the human body. Moreover, in both scenarios, the proposed antenna demonstrates strong matching characteristics and possesses an impressive impedance bandwidth spanning from 25.6 to 30.5 GHz (Hand) and 25.4 to 30.4 GHz (Biceps). These findings assure that relocating the antenna on the body won't drastically affect its

impedance bandwidth. The measured isolation is observed to be −27 dB at 26 GHz (Hand), and −29 dB at 26.2 GHz (Biceps). The gain and AR displayed in Fig. 14(c) exhibit a robust alignment between simulated and measured results, while the measured peak gain is determined to be 5.51 dBi, with an observed ARBW of 0.38 GHz, specifically ranging from 29.23 to 29.61 GHz. The far-field radiation characteristics ($\varphi = 0°$ and $\varphi = 90°$ planes) for the described antenna at two different frequencies are shown in Fig. 15. At 26.2 GHz the radiation beam is tilted to an angle $\theta = 300°$ in both planes which indicates the direction of maximum radiations. Whereas at 29.5 GHz the H-plane radiation beam is tilted at $\theta = 60°$, and the radiation in E-plane is toward the broadside direction.

MIMO diversity parameters

This section provides a thorough analysis of the diversity parameters associated with the proposed MIMO antenna system. Beyond the traditional antenna performance metrics, assessing a MIMO antenna system requires careful consideration of supplementary performance criteria to accurately define its diversity characteristics. These include the envelope correlation coefficient (ECC) which functions as a crucial performance metric, elucidating the degree of isolation or correlation present among communication channels. In the context of uncorrelated MIMO antenna systems, it is desirable for ECC to ideally be "0." However, practical implementations often yield ECC values frequently fall below the 0.5 threshold. Likewise, the performance analysis of a MIMO antenna system also incorporates the assessment of the diversity gain
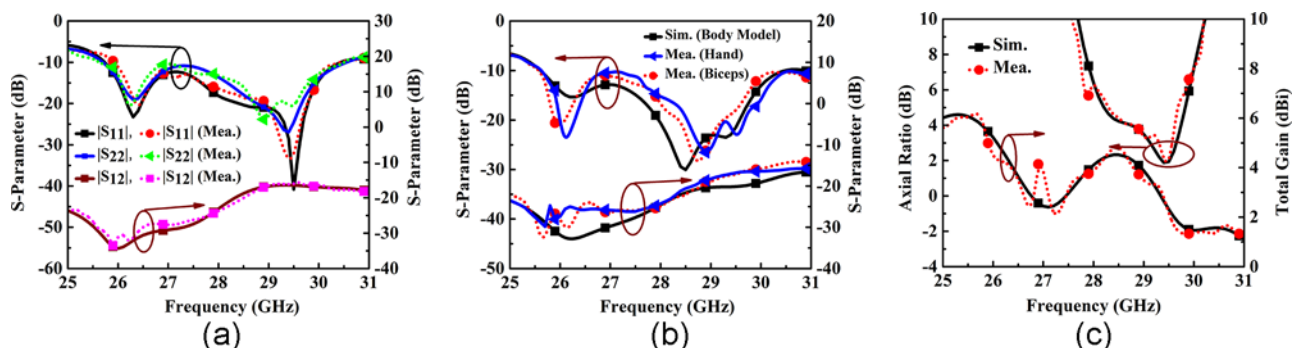
Figure 14. Simulated and measured performances analysis (a) S-parameter in free space, (b) S-parameter in human body, (c) Total gain and axial ratio.
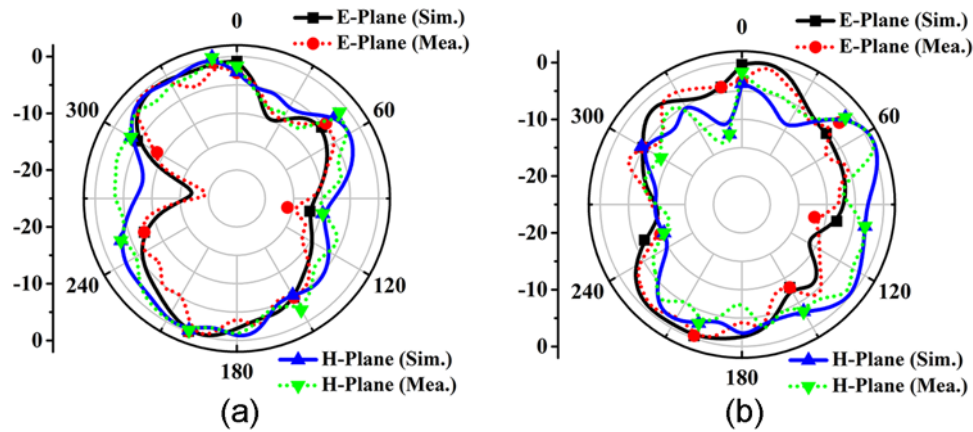
Figure 15. Radiation characteristics (far-field) (a) 26.2 GHz, (b) 29.5 GHz.
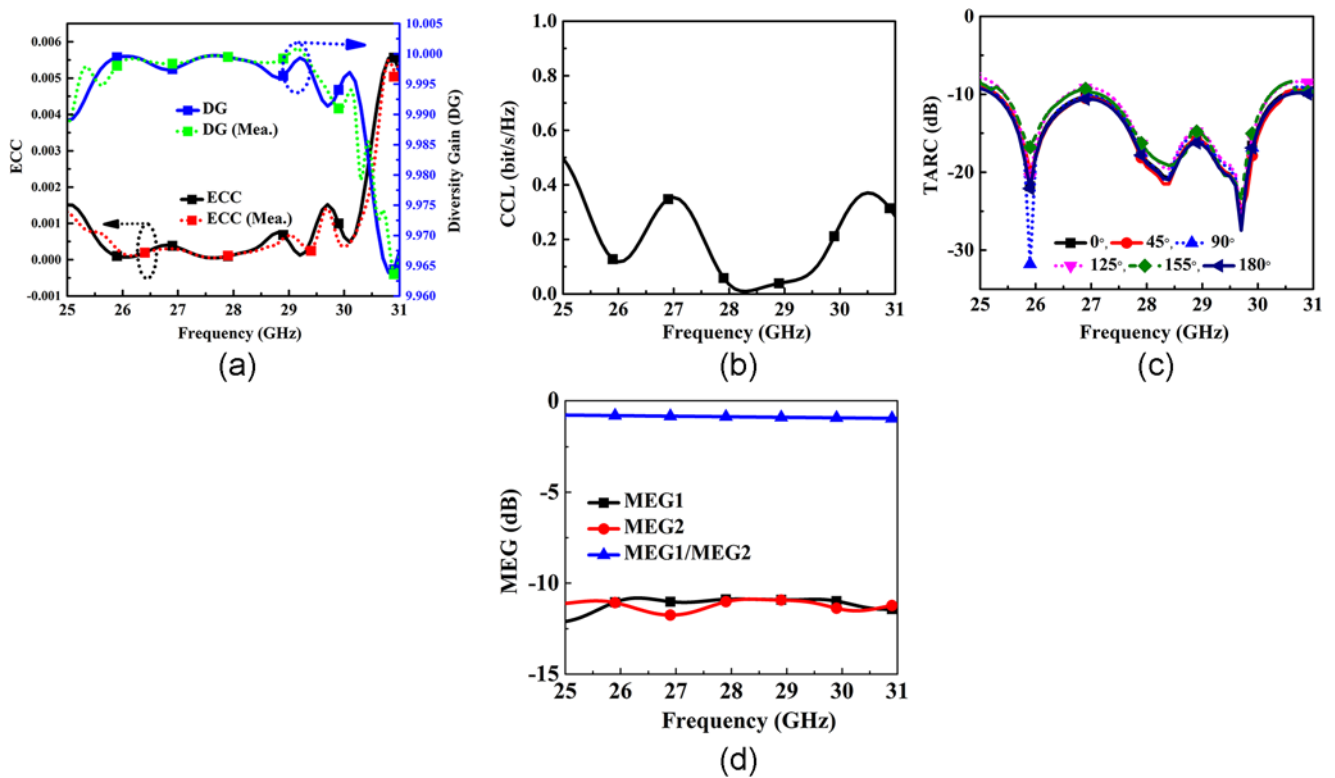
Figure 16. Diversity parameters (a) ECC and DG, (b) CCL, (c) TARC, (d) MEG.

(DG) parameter. This value can be calculated utilizing the S-parameters of each antenna element, employing the universal equations (2, 3) [38–40].

$$ECC = \frac{|S_{11}^* S_{12} + S_{21}^* S_{22}|^2}{(1 - (|S_{11}|^2 - |S_{21}|^2))(1 - (|S_{22}|^2 + |S_{12}|^2))} \quad (2)$$

$$DG = 10\sqrt{1 - |ECC|^2} \quad (3)$$

The simulated and measured ECC and DG across a frequency range of 25–31 GHz is observed to be approximately <0.001 and 9.99 as illustrated in Fig. 16(a). Likewise, channel capacity loss (CCL) constitutes a crucial metric within diversity analysis. This signifies the optimal transmission of EM signals capable of achieving the highest possible data rate between the transmitter and

receiver while minimizing distortion. Utilizing equations (4–6) the values of CCL can be computed.

$$C_{Loss} = -Log_2\left(|\Psi^R|\right) \quad (4)$$

$$\Psi^R = \begin{bmatrix} a_{11} & a_{12} \\ a_{21} & a_{22} \end{bmatrix} \quad (5)$$

$$a_{ij} = -\left[S_{11}^* S_{12} + S_{21}^* S_{12}\right] \quad (6)$$

The measured value from Fig. 16(b) is determined to be less than 0.4 bits/s/Hz, thereby falling within an acceptable range. The total active reflection coefficient (TARC) is also a crucial parameter in MIMO antenna system. This refers to the fluctuation in the

Table 2. Comparative performance analysis of the proposed MIMO antenna with the existing literature

Ref.	Substrate.material	No. of ports	Size (mm³)	Size red. (%)	BW (GHz)	Gain (dBi)	$\|S_{ij}\|$ (dB)	CP
[15]	Leather	2	35×52×2(=3640)	>89	5.8	4.1	27	No
[16]	Felt	2	38.1×38.1×2(=2903)	>87	0.1	2.79	12	No
[17]	Polyethylene foam	4	92×92×1.5(=12696)	>97	12	7.2	15	No
[18]	LCP	4	56×56×0.1(=313)	<16	1.02, 0.693.48	1.8, 2.63.7	20	No
[19]	Textile	4	55×58×1.4(=4466)	>91	1.2	>2	19	No
[22]	Textile	2	60×60×15(=54000)	>99	2.1	>4	22	Yes
[23]	Rogers 5880	2	30×30.5×0.254(=232)	<57	5.7	5.84	25	Yes
[24]	Textile	2	42×32.5×1.43(=1951)	>81	9.4	5.7	18	Yes
[25]	FR4	4	40×40×1.6(=2560)	>85	2.23	2.36	24	Yes
[26]	Rogers 5880	2	120×60×0.8(=5760)	>93	1.2	4	25	Yes
[27]	Rogers RO3003	4	32×18.5×0.25(=148)	<146	1.31.85	7.93.6	25	Yes
[28]	Rogers RO4350	2	68×80×0.8(=4352)	>91	4.6, 1.61.1, 7.5	10.1, 12.013.0, 5.55	29.5, 53.245.5, 43.6	No
[29]	Rogers 6002	2	19×15×0.254(=72)	<406	0.8	6	37	No
[30]	Rogers 5880	2	36×22.5×0.508(=405)	>9	7	4	25	Yes
[31]	Polyimide	4	NA	NA	7.8	8.9	22.5	No
This work	Rogers 5880	**2**	**32×20×0.508(=365)**	–	**4.9**	**5.6**	**>30**	Yes

BW: bandwidth, CP: circular polarization, NA: not available.

reflection coefficient caused by alterations in the phase angle of the signal introduced into the port. Mathematically it can be expressed using equation (7) [41].

$$TARC = \sqrt{\frac{|S_{11} + S_{12}e^{j\theta}|^2 + |S_{21} + S_{22}e^{j\theta}|^2}{2}} \qquad (7)$$

$$MEG1 = 0.5[1 - |S_{11}|^2 - |S_{12}|^2] \qquad (8)$$

$$MEG2 = 0.5[1 - |S_{12}|^2 - |S_{22}|^2] \qquad (9)$$

$$MEG = MEG1/MEG2 \qquad (10)$$

Figure 16(c) shows the computed TARC value for the designed antenna. The input signal phase is systematically adjusted in increments of 45°, spanning from 0° to 180°. In all phase angles the TARC value is observed to be consistently remains below −10 dB across the entire operating frequency range. Similarly, mean effective gain (MEG) is a crucial metric in diversity analysis, measuring the ratio of the average power received by the antenna under test to that of a reference antenna in the same environment. Equations (8–10) represents the general equation to calculate the MEG [19]. Figure 16(d) presents the MEG for port 1 (MEG1) and port 2 (MEG2), along with their difference (MEG1/MEG2). It is clear that the MEG ratio remains below −3 dB. A comparative analysis is carried out between the proposed antenna and findings from existing literature, as summarized in Table 2. It is observed that the designed MIMO antenna system presented in references [15–17, 19, 22–26, 30, 31] exhibits a large circuital area, although, the operating bandwidth in references [23, 24, 30] is quite good compared to the proposed MIMO antenna design. Subsequently the antenna gain in references [17, 24, 28, 29, 31] is high. It is further observed that the presented antenna in references [18, 27, 29]

features compact dimensions but fails to achieve optimal performance in terms of operating bandwidth, gain, isolation, and CP characteristics. Beside the analysis of performance behavior using the CMT is missing. In contrast, the proposed work introduces a novel circularly polarized dual-port MIMO antenna, which has been designed, fabricated, and thoroughly investigated using the theory of characteristic modes. The proposed antenna structure demonstrates acceptable performance characteristics, making it suitable for body-worn applications in the millimeter-wave frequency bands.

Conclusion

Dual element MIMO antenna system with circularly polarized radiation behavior is successfully designed and validated through experimental analysis. The antenna design incorporates two flower-shaped radiators arranged in a spatial diversity configuration. The ground layer has been modified through the incorporation of dual crescent-shaped slots, facilitating an extensive frequency band of operation spanning from 25.7 to 30.6 GHz. The truncation in the ground layer results in offering CP at 29.4 GHz with a 3-dB ARBW of 0.6 GHz (29.1–29.7 GHz). The attainment of CP within the antenna structure has been substantiated via analysis through CMT. A total gain of 5.6 dBi has been achieved, accompanied by a port isolation of −34 dB. Additionally, comprehensive validation of diversity metrics, such as ECC, DG, CCL, and TARC, has been conducted. Furthermore, the antenna is subject to thorough analysis to evaluate its performance in bending conditions and SAR, in order to ensure its suitability for body-worn applications in biotechnologies.

Competing interests. The authors report no conflict of interest.

References

1. **Sundarsingh EF, Kanagasabai M and Ramalingam VS** (2017) Completely integrated multilayered weave electro-textile antenna for wearable applications. *International Journal of Microwave and Wireless Technologies* **9**(10), 2029–2036.
2. **Sid A, Cresson PY, Joly N, Braud F and Lasri T** (2022) A flexible and wearable dual band bio-based antenna for WBAN applications. *AEU - International Journal of Electronics and Communications* **157**, 1–9.
3. **Kiourti A** (2018) RFID antennas for body-area applications: From wearables to implants. *IEEE Antennas and Propagation Magazine* **60**(5), 14–25.
4. **Varkiani SMH and Afsahi M** (2019) Compact and ultra-wideband CPW-fed square slot antenna for wearable applications. *AEU - International Journal of Electronics and Communications* **106**, 1–8
5. **Ur-Rehman M, Malik NA, Yang X, Abbasi QH, Zhang Z and Zhao N** (2017) A low profile antenna for millimeter-wave body-centric applications. *IEEE Transactions on Antennas and Propagation*, **65**(12), 6329–6337.
6. **Paracha KN, Abdul Rahim SK, Soh PJ and Khalily M** (2019) Wearable antennas: A review of materials, structures, and innovative features for autonomous communication and sensing. *IEEE Access* **7**, 56694–56712.
7. **Dey AB, Kumar S, Arif W and Anguera J** (2023) Elastomeric textile substrates to design a compact, low-profile AMC-based antenna for medical and IoT applications. *IEEE Internet of Things Journal*, **10**(6), 4952–4969.
8. **Joshi JG, Pattnaik SS and Devi S** (2012) Metamaterial embedded wearable rectangular microstrip patch antenna. *International Journal of Antennas and Propagation* **2012**, 974315.
9. **Le TT and Yun TY** (2021) Wearable dual-band high-gain low-SAR antenna for off-body communication. *IEEE Antennas and Wireless Propagation Letters* **20**(7), 1175–1179.
10. **Zhao Z, Zhang C, Lu Z, Chu H, Chen S, Liu M and Li G** (2023) A miniaturized wearable antenna with five band-notched characteristics for medical applications. *IEEE Antennas and Wireless Propagation Letters* **22**(6), 1246–1250.
11. **Modak S, Kaim V, Khan T, Kanaujia BK, Matekovits L and Rambabu K** (2024) Design and performance measurement of worn-on-body instrumental ultra-miniaturized UWB wearable patch for e-health monitoring. *IEEE Access* **12**, 25719–25730.
12. **Faisal F, Amin Y, Cho Y and Yoo H** (2019) Compact and flexible novel wideband flower-shaped CPW-fed antennas for high data wireless applications. *IEEE Transactions on Antennas and Propagation* **67**(6), 4184–4188.
13. **Ashyap AYI, Abidin ZZ, Dahlan SH, Majid HA, Waddah AMA, Kamarudin MR, Oguntala GA, Alhameed RAA and Noras JM** (2018) Inverted E-shaped wearable textile antenna for medical applications. *IEEE Access* **6**, 35214–35222.
14. **Ferreira D, Pires P, Rodrigues R and Caldeirinha RFS** (2017) Wearable textile antennas: Examining the effect of bending on their performance. *IEEE Antennas and Propagation Magazine* **59**(3), 54–59.
15. **Pandey R, Biswas AK and Chakraborty U** (2023) Non-conventional leather substrate based high isolation wideband MIMO antenna for body-centric applications. *AEU - International Journal of Electronics and Communications* **170**, 1–14.
16. **Li H, Sun S, Wang B and Wu F** (2018) Design of compact single-layer textile MIMO antenna for wearable applications. *IEEE Transactions on Antennas and Propagation* **66**(6), 3136–3141.
17. **Jayant S, Srivastava G and Kumar S** (2022) Quad-port UWB MIMO footwear antenna for wearable applications. *IEEE Transactions on Antennas and Propagation* **70**(9), 7905–7913.
18. **Peng I and Du C** (2024) A flexible CPW-fed tri-band four-port MIMO antenna for 5G/WIFI 6E wearable applications. *AEU - International Journal of Electronics and Communications* **174**, 1–11.
19. **Roy S, Biswas AK, Ghosh S, Chakraborty U and Sarkhel A** (2021) Isolation improvement of dual-/quad-element textile MIMO antenna for 5G application. *Journal of Electromagnetic Waves and Applications* **35**(10), 1337–1353.
20. **Qu L, Piao H, Qu Y, Kim HH and Kim H** (2018) Circularly polarised MIMO ground radiation antennas for wearable devices. *Electronics Letters* **54**, 189–190.
21. **Modak S, Kaim V, Zaidi AM, Kanaujia BK and Rambabu K** (2024) Design of electrically small intraocular antenna for retinal prosthesis system and its validation. *IEEE Transactions on Biomedical Engineering* **71**(12), 3402–3412.
22. **Illahi U, Iqbal J, Ramey SM and Sulaiman MI** (2024) Design and development of a new circularly polarized MIMO wearable DRA for WBAN applications. *AEU - International Journal of Electronics and Communications* **177**, 1–9.
23. **Xu M and Zhang J** (2023) circularly polarized multiple-input multiple-output dielectric resonator antenna for 5G millimeter-wave application. *Electronics* **12**, 1–18.
24. **Kumar S, Nandan D, Srivastava K, Kumar S, Singh H, Marcy M, Mostafa H and Kanaujia BK** (2021) Wideband circularly polarized textile MIMO antenna for wearable applications. *IEEE Access* **9**, 108601–108613.
25. **Iqbal A, Smida A, Alazemi AJ, Waly MI, Khaddaj Mallat N and Kim S** (2020) Wideband circularly polarized MIMO antenna for high data wearable biotelemetric devices. *IEEE Access* **8**, 17935–17944.
26. **Dwivedi AK, Narayanaswamy NK, Penmatsa KKV, Singh SK, Sharma A and Singh V** (2023) Circularly polarized printed dual port MIMO antenna with polarization diversity optimized by machine learning approach for 5G NR n77/n78 frequency band applications. *Scientific Reports* **13**, 1–18.
27. **Alaal N, Elsayed RA, Farahat AE, Hussein KFA and Deeb WSE** (2024) Q-band MIMO antennas with circular polarization for spatial and polarization diversity. *Journal of Infrared, Millimeter, and Terahertz Waves* **45**, 393–432.
28. **Kumar A, Pattanayak P, Verma RK, Sabat D and Prasad G** (2023) Two-element MIMO antenna system for multiband millimeter-wave, 5G mobile communication, Ka-band, and future 6G applications with SAR analysis. *AEU - International Journal of Electronics and Communications* **171**, 1–14.
29. **Iqbal A, Basir A, Smida A, Mallot NK, Elfergani I, Rodriguez J and kim S** (2019) Electromagnetic bandgap backed millimeter-wave MIMO antenna for wearable applications. *IEEE Access* **7**, 111135–111144.
30. **Tiwari RN, Kaim V, Singh P, Khan T and Kanaujia BK** (2023) Semi-flexible diversified circularly polarized millimeter-wave MIMO antenna for wearable biotechnologies. *IEEE Transactions on Antennas and Propagation* **71**(5), 3968–3982.
31. **Shariff BGP, Ali T, Mane R, Alslath MGN, Kumar P, Pathan S, Kishk AA and Khan T** (2024) Design and measurement of a compact millimeter wave highly flexible MIMO antenna loaded with metamaterial reflective surface for wearable applications. *IEEE Access* **12**, 30066–30084.
32. **Balanis CA** (1997) *Antenna Theory – Analysis and Design, Chap. 14*. Hoboken, New Jersey: John Wiley & Sons, pp. 1–1146.
33. **Modak S, Lokam A and Farooq U** (2024) Characteristic mode based self isolated MIMO antenna design for millimeter wave 5G communications. *AEU - International Journal of Electronics and Communications* **178**, 1–11.
34. **Modak S, Khan T and Laskar RH** (2020) Penta-notched UWB monopole antenna using EBG structures and fork-shaped slots. *Radio Science* **55**, 1–11.
35. **Modak S, Daasari S, Shome PP and Khan T** (2023) Switchable/tunable band-notched characteristics in UWB and UWB-MIMO antennas: A comprehensive review. *Wireless Personal Communications* **128**, 2131–2154.
36. **Han M and Dou W** (2019) Compact clock-shaped broadband circularly polarized antenna based on characteristic mode analysis. *IEEE Access* **7**, 159952–159959.
37. **Sharma A, Gangwar D, Singh RP, Solanki R, Rajpoot S, Kanaujia BK, Singh SP and Ekuakille AL** (2021) Design of compact wideband circularly polarized hexagon-shaped antenna using characteristics mode analysis. *IEEE Transactions on Instrumentation and Measurement* **70**, 1–8.
38. **Modak S and Khan T** (2021) A slotted UWB-MIMO antenna with quadruple band-notch characteristics using mushroom EBG structure. *AEU - International Journal of Electronics and Communications* **134**, 1–6.
39. **Farooq U and Lokam A** (2023) A compact 26/39 GHz millimeter wave MIMO antenna design for 5G IoT applications. *Journal of Infrared, Millimeter, and Terahertz Waves* **44**, 333–345.

40. **Modak S and Khan T** (2021) Cuboidal quad-port UWB-MIMO antenna with WLAN rejection using spiral EBG structures. *International Journal of Microwave and Wireless Technologies*, **14**(5), 626–633.

41. **Eslami A, Nourinia J, Ghobadi C and Shokri M** (2021) Four-element MIMO antenna for X-band applications. *International Journal of Microwave and Wireless Technologies* **13**(8), 859–866.

Sumon Modak (Member, IEEE) received the B. Tech. degree in electronics and communication engineering from Dr. M. G. R. University (A Deemed University), Chennai, Tamil Nadu, India, the M. Tech. degree in communication system engineering from Sambalpur University (SUIIT), Sambalpur, Odisha, India, and the Ph.D. degree in electronics and communication engineering from the National Institute of Technology Silchar, Assam, India. He is currently a Postdoctoral Fellow with the Department of Electronics and Communication Engineering, National Institute of Technology Warangal, Telangana, India. His current research interests include UWB and millimeter-wave antennas, EBG structures, CMA, and implantable antenna for biomedical applications.

Prof L.Anjaneyulu obtained his B.Tech (ECE) in 1989, M.Tech from R.E.C (N.I.T), Warangal in 1991 and Ph.D from N.I.T, Warangal in 2009. He worked as Project Officer at Institute of Armament Technology (DRDO), Pune, India for 5 years from 1991 and involved in the design of Surface borne and Air-borne Radar systems for clutter measurement application. Later, he worked as Staff Scientist at Helios Systems, Madras, India for 2 years from 1995 and engaged in the development of Radio Wave propagation assessment software modules for ship-borne radars of Indian Navy. He has been with the department of Electronics and communications engineering at National Institute of Technology, Warangal, India since 1997 and has 25 years of teaching experience. He is presently working as Professor in the department. He has completed few defence R&D Projects from DRDO and ISRO and has around 100 papers to his credit in National and International Conferences and journals. He is a senior member of IEEE, IEEE-APS, Life member of ISTE, Fellow of Institute of Engineers, Fellow of IETE.

Umar Farooq is currently working as an Assistant Professor at VNR Vignana Jyothi Institute of Technology Hyderabad, India. He received his B. Tech. degree in Electronics and Communication Engineering from Islamic University of Science and Technology, Kashmir, India, in 2012, M. Tech. degree from Government Engineering College Bathinda, Punjab, India in 2014 and Ph.D. degree from National Institute of Technology (NIT) Srinagar, India in 2020. He has also worked as Assistant Professor in National Institute of Technology Srinagar, India and Lecturer in Islamic University of Science and Technology, Kashmir, India. He is a member of IEEE, IEI, IAENG, and IIETA. His research interests include Wireless Sensor Networks, Internet of Things, Millimeter and Terahertz Communication, Antenna design.